STScI | SPACE TELESCOPE SCIENCE INSTITUTE

# JWST TECHNICAL REPORT

| | |
|---|---|
| Title: NIRISS Commissioning Results: NIS-022 – NIRISS PSF Characterization (NGAS CAR-706, APT 1096) | Doc #: JWST-STScI-008324<br>Date: 6 December 2022<br>Rev: - |
| Authors: Paul Goudfrooij, Swara Ravindranath, and the NIRISS team Phone: 4981 | Release Date: 15 December 2022 |

## 1 Abstract

This report presents analysis and results of commissioning program NIS-022 (NGAS CAR-706, APT 1096). We describe the data and analysis used to characterize the NIRISS imaging PSF for all NIRISS filters in terms of encircled and ensquared energy as a function of distance from the star and stellar FWHM and ellipticity, and the variation of those properties across the NIRISS field of view.

## 2 Introduction

The imaging data was obtained in 3 visits during May 14-15, 2022, using APT program 1096. The target for the first two visits was SDSS J125701.95+220415.5, a star with SDSS z magnitude 18.45, for which predictions with the pre-launch ETC indicated that it should not saturate for at least 3 groups up the ramp, even for broad-band NIRISS filters with short pivot wavelengths such as F090W and F115W, which have the highest sensitivity. The field around this star, which is shown in Figure 1, was purposely chosen to be sparse to allow a characterization of the outskirts of the PSF without running into crowding issues. We used an OFFSET special requirement so as to place the nearby star SDSS J125659.56+220511.3 (z = 15.6) also comfortably within the NIRISS field of view so that both stars could be used if necessary and deemed useful. For visit #1, we cycled through all broad-band filters and the short-wavelength medium-band filters and we restricted the allowed range of aperture position angles in APT such that both stars would be placed in relatively "clean" areas on the detector in terms of bad pixels and flat field quality. For visit #2, we placed SDSS J125701.95+220415.5 near the four detector corners using a 2x2 mosaic, using 3 of the filters in order to allow a characterization of the PSF properties across the field of view.
To reach similar S/N in the medium-band filters with the longest pivot wavelengths (i.e., F380M, F430M, and F480M), we observed the bright CALSPEC flux standard GD153 (K = 14.3, a hot white dwarf) in a separate visit (#3). The data files and exposure specifications are listed in Table 1 below. Numbers of groups per integration were determined using the JWST ETC, and chosen to reach roughly three times the saturation level in the peak pixel, thus allowing one to image the outskirts of the PSF at high enough S/N. All exposures were done using a 2-point dither pattern.

The following analysis was performed on the _cal.fits data products from JWST calibration pipeline version 1.5.0, using CRDS context jwst_0831.pmap.

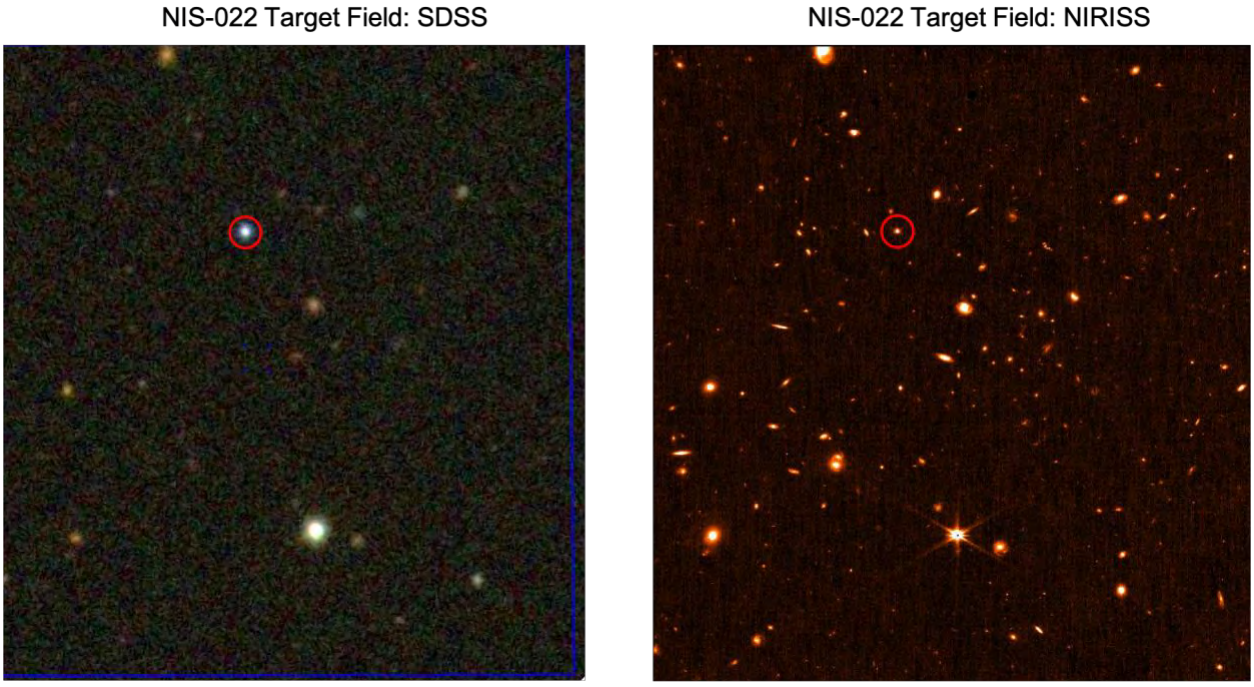


**Figure 1: NIS-022 target field. Left panel shows the Sloan Digital Sky Survey (SDSS) image, while the right panel shows the NIRISS F200W image. For reference, target SDSS J125701.95+220415.5 is encircled in red.**

**Table 1: Properties of exposures from APT program 1096 used for this analysis. The Readout Pattern was NISRAPID in all cases.**

| FITS file root ID | Target | Subarray | Pupil | Filter | Dithers | NGROUPS | NINTS |
|---|---|---|---|---|---|---|---|
| **Observation / Visit 1** | | | | | | | |
| jw01096001001_02101 | J125701.95+220415.5 | FULL | F200W | CLEAR | 2 | 8 | 1 |
| jw01096001001_02103 | J125701.95+220415.5 | FULL | F150W | CLEAR | 2 | 8 | 1 |
| jw01096001001_02105 | J125701.95+220415.5 | FULL | F140M | CLEAR | 2 | 14 | 1 |
| jw01096001001_02107 | J125701.95+220415.5 | FULL | F158M | CLEAR | 2 | 14 | 1 |
| jw01096001001_02109 | J125701.95+220415.5 | FULL | F115W | CLEAR | 2 | 8 | 1 |
| jw01096001001_0210b | J125701.95+220415.5 | FULL | F090W | CLEAR | 2 | 10 | 1 |
| jw01096001001_0210d | J125701.95+220415.5 | FULL | CLEARP | F277W | 2 | 12 | 1 |
| jw01096001001_0210f | J125701.95+220415.5 | FULL | CLEARP | F444W | 2 | 8 | 1 |
| jw01096001001_0210h | J125701.95+220415.5 | FULL | CLEARP | F356W | 2 | 18 | 1 |
| **Observation / Visit 2** | | | | | | | |
| jw01096002001_02101 | J125701.95+220415.5 | FULL | F200W | CLEAR | 2 | 8 | 1 |
| jw01096002001_02103 | J125701.95+220415.5 | FULL | F115W | CLEAR | 2 | 8 | 1 |
| jw01096002001_02105 | J125701.95+220415.5 | FULL | CLEARP | F356W | 2 | 18 | 1 |
| jw01096002002_02101 | J125701.95+220415.5 | FULL | F200W | CLEAR | 2 | 8 | 1 |
| jw01096002002_02103 | J125701.95+220415.5 | FULL | F115W | CLEAR | 2 | 8 | 1 |
| jw01096002002_02105 | J125701.95+220415.5 | FULL | CLEARP | F356W | 2 | 18 | 1 |
| jw01096002003_02101 | J125701.95+220415.5 | FULL | F200W | CLEAR | 2 | 8 | 1 |
| jw01096002003_02103 | J125701.95+220415.5 | FULL | F115W | CLEAR | 2 | 8 | 1 |

| FITS file root ID | Target | Subarray | Pupil | Filter | Dithers | NGROUPS | NINTS |
|---|---|---|---|---|---|---|---|
| jw01096002003_02105 | J125701.95+220415.5 | FULL | CLEARP | F356W | 2 | 18 | 1 |
| jw01096002004_02101 | J125701.95+220415.5 | FULL | F200W | CLEAR | 2 | 8 | 1 |
| jw01096002004_02103 | J125701.95+220415.5 | FULL | F115W | CLEAR | 2 | 8 | 1 |
| jw01096002004_02105 | J125701.95+220415.5 | FULL | CLEARP | F356W | 2 | 18 | 1 |
| **Observation / Visit 3** | | | | | | | |
| jw01096003001_02101 | GD-153 | FULL | CLEARP | F430M | 2 | 38 | 1 |
| jw01096003001_02103 | GD-153 | FULL | CLEARP | F380M | 2 | 20 | 1 |
| jw01096003001_02105 | GD-153 | FULL | CLEARP | F480M | 2 | 52 | 1 |

## 3 Aperture Photometry

Multi-aperture photometry was performed using scripts in the nis_comm/nis_022 folder of the NIRISS Commissioning repository on GitHub (https://github.com/spacetelescope/niriss-commissioning). The main functions used here are pgphotdefs.pgphotdit2 (for circular apertures) and pgphotdefs_sq.pgphotdit2 (for square apertures) along with wrapper scripts that manage output file names and the aperture radii for the measurements. The main steps performed can be summarized as follows:

1. Read in the _cal.fits files (i.e., the level-2 products of the JWST pipeline), then divide the science extensions by the value of header keyword PHOTMJSR so as to obtain flat-fielded count rate images in units of ADU/s.
2. Establish high-precision center positions for the target star in the two dither positions. To this end, the position of the star in the different dithers was first estimated from the XOFFSET and YOFFSET header keywords translated to positions in the "science" (DMS) coordinate frame using script idealdithers.py. This was followed by a 2-D Gaussian fit (photutils.centroids.centroid_2dg) with a box size of $9 \times 9$ pixels, which method was recently shown to provide the most robust and precise centroids for undersampled NIRISS PSFs (Goudfrooij 2022).
3. Determine a clipped mean background level for each image and subtract it, so as to obtain 2 dithered images (per filter) with the same (zero) background level.
4. Using the DQ arrays, identify bad (though not saturated) pixels around the target in each image using X and Y positions relative to that of the location of the target. If a pixel is bad in only one of the two dithers, replace its value by that in the other dither (using that target-centered coordinate system). If a pixel is bad in both dithers, replace it by means of 2-D interpolation using its neighbors. (Note: This step is only done outside a radius of 5 pixels.)
5. For each of the two images, use $\kappa$-$\sigma$ clipping statistics in the sky measurement region to determine the signal threshold below which (anomalously low) sky values be clipped out of the range used to calculate statistics. This step was shown by Goudfrooij et al. (2022) to be important for data taken with some of NIRISS subarrays, for which several pixels with significantly negative values were present around the source regions in the case of short exposures. However, the impact of this step turned out to be only marginal for the positions

of the targets in the NIS-022 exposures.

6. Add the background levels found in step 3 above back into the images.
7. Perform multi-aperture photometry using photutils.aperture_photometry. For the purpose of the measurements for NIS-022, we used the following aperture radii: [0.7,1,1.54,2,2.5,2.72,3,4,5,6,7,8,9,10,12,14,16,18,20,22,24,26,28,30,35,40,45,50,55,60,65,70] to measure encircled energies (hereafter EEs). The radii of 1.54, 2.50, and 2.72 pixels were included as they correspond to the first minimum of the Airy pattern convolved with the pixel size of the NIRISS detector for certain filters, and EE measurements for those radii were used in judging imaging science readiness during commissioning. For the *ensquared* energy (hereafter EsqE) measurements, we used the following widths: [3,5,7,9,11,13,15,17,19,21,25,31,35,41,45,51,55,61,65,71,75,81,85,91]. Sky background measurements were made using κ-σ clipping statistics in a 5-pixel wide annulus with an inner edge starting 10 pixels outside of the outermost object measurement aperture.
8. Calculate object and sky counts in electrons per integration in order to calculate proper photometric errors, and calculate fluxes and their errors in units of electrons/s. We assume a gain of 1.61 electrons/ADU for the NIRISS detector in this step. (Note: this step is not needed for encircled or ensquared energy measurements, but it is part of the pgphotdit2 function nonetheless.)
9. Combine the measurements from the two dithers into one file per filter, and calculate weighted average fluxes at each aperture size.

For the determination of aperture corrections, we also created images using WebbPSF (Perrin et al. 2012, 2014) for each filter and dither position, using the exact same center positions as those found for the observed star, an oversampling factor of 11, and a size of 301×301 pixels with the native NIRISS pixel size. For this purpose, WebbPSF was used with the pre-launch optical path difference file, since WebbPSF wasn't updated with on-orbit results until well after commissioning. This step is done using script mkwebbPSFs.py, using the output files from step 7 above as input. Note that these WebbPSF output images are normalized to an integrated flux of unity in the process. We then repeated steps 2 and 7-9 above for those PSF images to obtain the aperture corrections, making sure that the fractions of the PSF's source flux in the sky annulus are also accounted for.

The aperture corrections were applied to the aperture photometry of the target stars using script EEnormalize_nis.py or EEnormalize_nis_sq.py, which apply the aperture correction by multiplying the observed fluxes by the average ratio "EE (PSF) / EE (star)" or "EsqE (PSF) / EsqE (star)" for a given filter within a specified range of aperture radii or widths. After some experimentation, we chose a range in radius from 9 to 16 pixels for this "normalization" for EEs (and a range in widths of 17-31 pixels for EsqEs). These radii and widths are large enough to avoid the dependency on precise centering of undersampled PSFs relative to pixel borders. This dependency is significant

for small apertures, as can be appreciated from Figure 2 which shows EEs for the various filters for each dither separately (note that the two dithers differ in pixel phase by 0.5 pixel in X and Y). The outer edge of the normalization region also avoids relatively large photometric uncertainties due to the low surface brightness of the target star at larger distances.

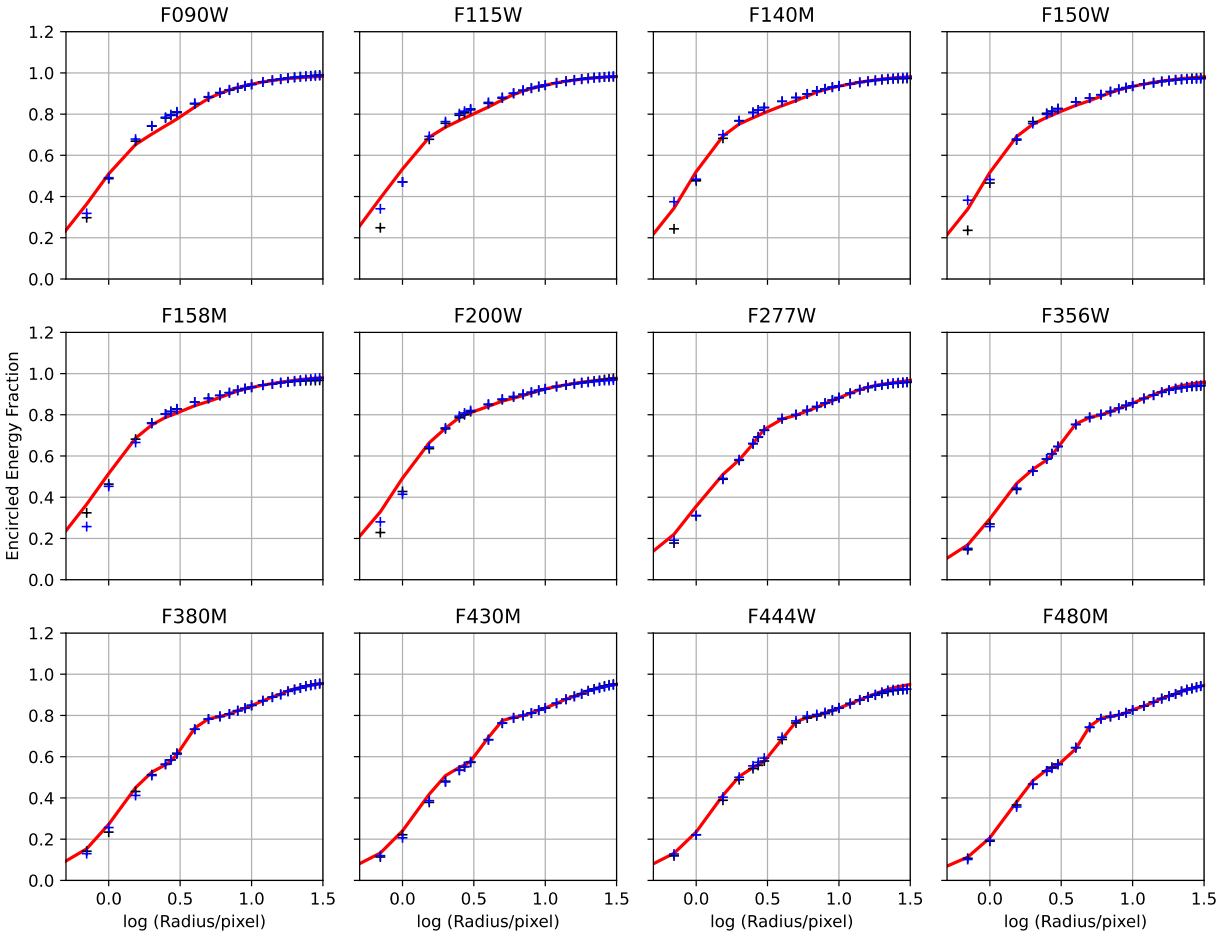


**Figure 2: encircled energy curves from NIS-22. Filters are mentioned at the top of each panel. Data points represent photometry of J125701.95+220415.5 or GD 153, normalized by the averaged photometry of WebbPSF images, placed at the same positions as the star, at large radii. Blue and black symbols represent measurements from level-2 pipeline products (i.e., the _cal.fits files) of each of the two dithers. The WebbPSF photometry is shown as a red line in each panel. Note the differences between the dithers at the smallest radii for the short-wavelength filters, whose PSFs are heavily undersampled.**

# 4 Results

## 4.1 Encircled and Ensquared Energy

Tables with results on EEs and EsqEs for visits 1 and 3 of NIS-22 have been made available on stsci.box.com in folder https://stsci.box.com/s/50bno6qfr8yas1y79wvf96yghkbh5nq1. The tables are in ascii format and are called NIS22_normEE.dat and NIS22_normEsqE.dat. The first line in each

table lists the columns with self-explanatory names: Radius (or width), and EE (or EsqE) for every NIRISS filter and their uncertainties. These results are depicted in Figures 3 and 4, and some highlights are described below.

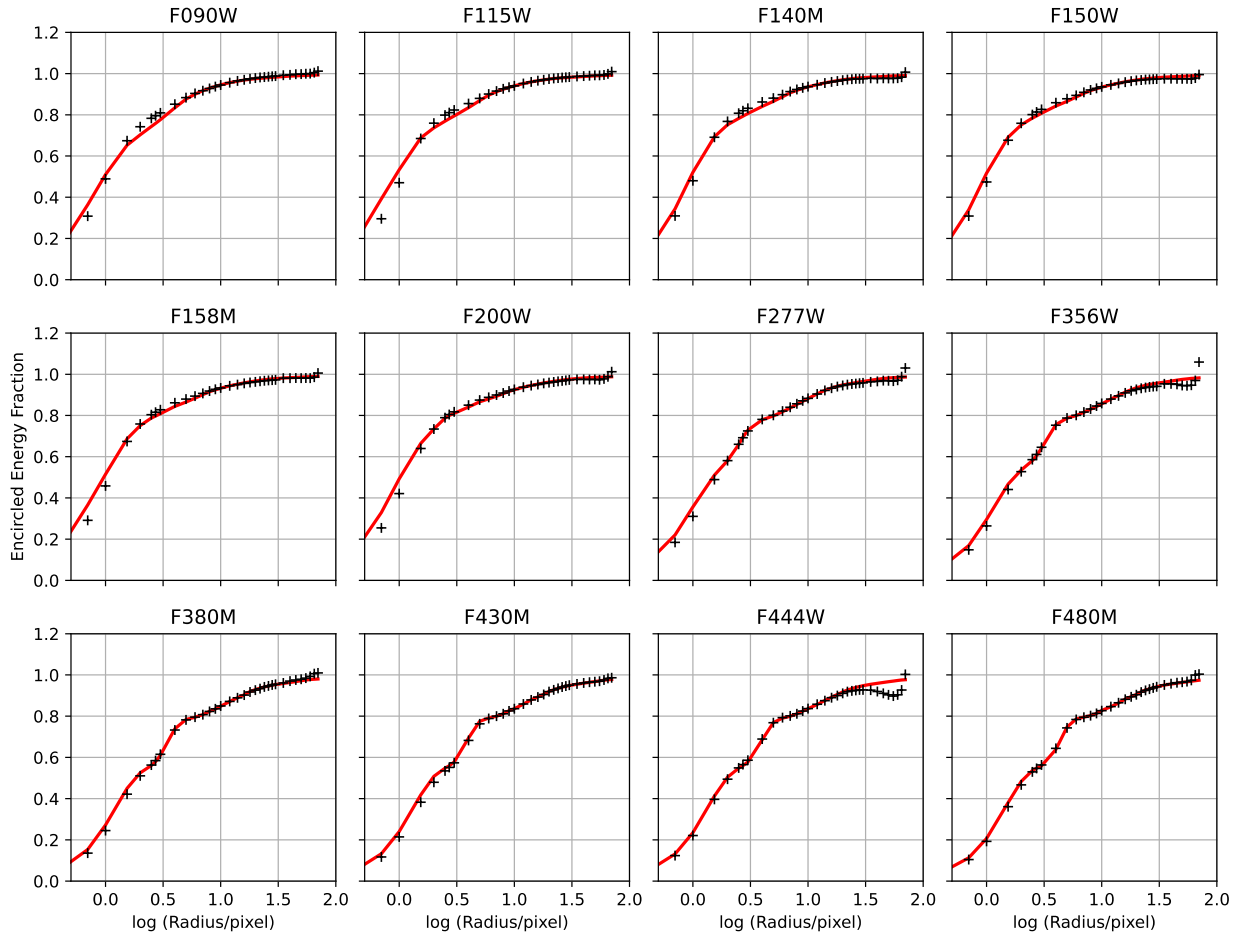


**Figure 3: similar to Figure 2, but over a larger range in radius, and the data points now represent aperture photometry for each filter after averaging over the two dithers.**

Comparing the results with the pre-launch WebbPSF predictions, we see that the EE values for filters with pivot wavelength ≥ 2 μm agree very well with the pre-launch predictions except for slight deviations at radii ≥ 30 pixels for filters F356W and F444W. It is likely that the latter deviations are due to uncertainties related to sky subtraction, since the S/N ratios of the exposures with those two filters were the lowest of all. At shorter wavelengths, we see that the EE values for filters F090W, F115W, F140M, F150W, and F158M are systematically somewhat higher than the WebbPSF predictions at radii of 2 – 6 pixels (or box widths of 3 – 12 pixels), indicating a PSF that is more centrally peaked than the pre-launch prediction. While this isn't the case for radii ≤ 1 pixel in Figure 3, Figure 2 showed that EE values for such small radii are strongly dependent on centroid placement relative to pixel boundaries, and two dithers per filter does not provide sufficient statistics on this aspect, so we do not assign much weight on this for now. This will be revisited once additional EE measurements have been analyzed from Cycle 1 calibration programs.

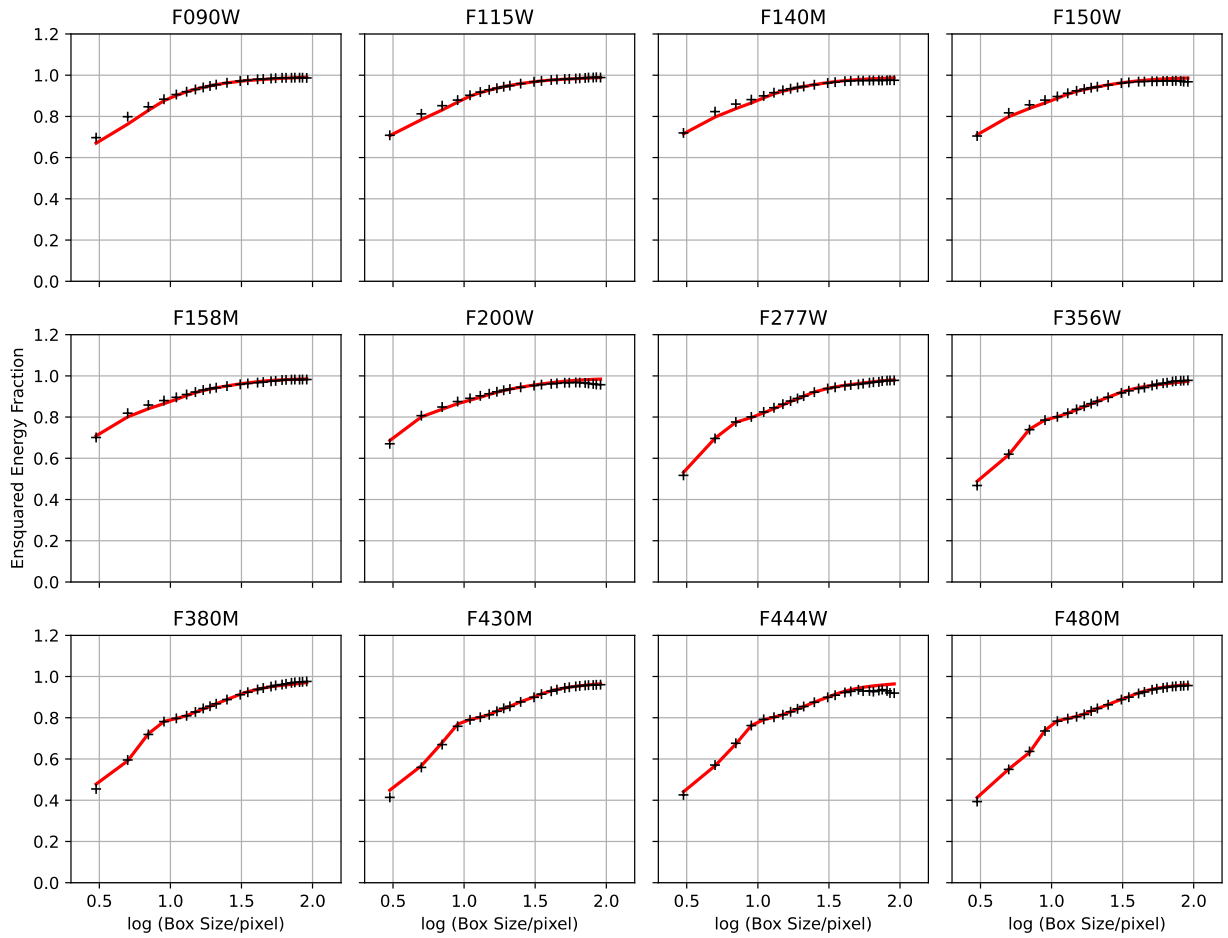


**Figure 4: similar to Figure 3, but now showing *ensquared* energy fraction as a function of measurement box width.**

## 4.2 FWHM

FWHM measurements of the target star were made for each individual _cal.fits image and each WebbPSF image created as described in §3, using an implementation of the psfmeasure task in IRAF which measures "direct" FWHMs without the assumption of a functional form of the PSF. After averaging over the two dithers per filter, the FWHM measurements are tabulated and depicted in Figure 5. As might have been expected from the EE results described above, the FWHM values of the NIS-022 PSFs are consistent with average values of a large set of pre-launch WebbPSFs that were resampled onto the native NIRISS pixel array.

| Filter | FWHM (NIS-022) | FWHM (WebbPSF) |
|---|---|---|
| F090W | 1.33 ± 0.08 | 1.45 |
| F115W | 1.42 ± 0.08 | 1.39 |
| F140M | 1.39 ± 0.14 | 1.39 |
| F150W | 1.39 ± 0.18 | 1.39 |
| F158M | 1.44 ± 0.08 | 1.39 |
| F200W | 1.61 ± 0.10 | 1.42 |
| F277W | 1.73 ± 0.07 | 1.67 |
| F356W | 1.99 ± 0.04 | 1.92 |
| F380M | 2.11 ± 0.03 | 2.06 |
| F430M | 2.28 ± 0.02 | 2.27 |
| F444W | 2.24 ± 0.04 | 2.28 |
| F480M | 2.54 ± 0.02 | 2.53 |

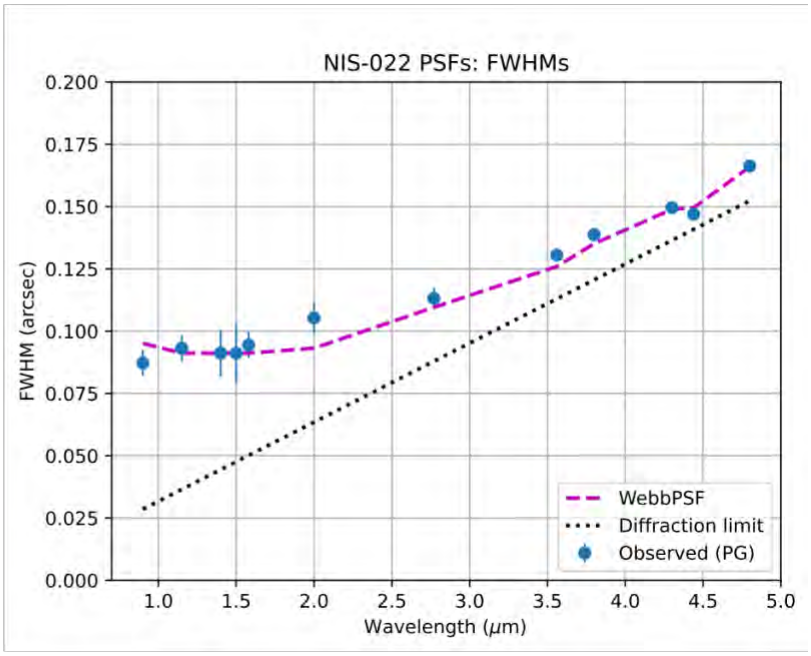


**Figure 5: NIRISS PSF FWHM as function of filter pivot wavelength. Measured FWHMs for the level-2 pipeline products of the NIS-022 data are listed on the left and represented by blue circles in the Figure. For comparison, the magenta dashed line represents measured FWHMs of pre-launch WebbPSF models resampled onto the native NIRISS pixel array, and the black dotted line indicates the theoretical diffraction limit for JWST.**

## 5 Field dependence of EE and FWHM

To characterize the field dependence of the PSF we used the data from observation #2 of the NIS-022 program which were obtained by placing the star SDSS J125701.95+220415.5 near the center and at the four detector corners using a 2x2 mosaic (i.e., 4 JWST visits). The observations used 3 filters (F115W, F200W, and F356W) to cover a broad range of wavelengths and obtain the representative PSF variation across the detector. Unfortunately, the visit with the star placed at the lower right corner of the detector failed and was not repeated. FWHM and ellipticity measurements of the PSF at the different spatial locations were done using the IRAF *imexamine* task and are listed in Table 2. The FWHM is the direct measure of the radius (multiplied by 2) at which the intensity reaches half the peak value, and the ellipticity is calculated from the second intensity moments. The ellipticity changes are not significant across the detector and the FWHM (in pixels) only vary by 5 – 8 % across the detector in the range of wavelengths covered by the 3 filters.

The encircled energy for the different locations were measured on the individual images using the *nispsfs.nisapphot* python code, available in the GitHub link provided in Section 3. The centroid determination uses the *photutils.centroid_2dg* function, and the photometry is done using the CircularAperture photometry function in photutils. The resulting EE curves are shown in Figure 6. For comparison, the EE profile of the WebbPSF generated for the center position is also shown. The encircled energy curves for the different positions across the detector match very well for large radii (≥ 2 pixels from the PSF center) in all filters.

**Table 2: Measured Ellipticity and FWHM across different locations on the NIRISS detector.**

| Filter | Quadrant on the detector | Ellipticity | FWHM (pixels) |
|---|---|---|---|
| F115W | Center | 0.04 +/- 0.00 | 1.35 +/- 0.02 |
| | Upper right | 0.03 +/- 0.00 | 1.41 +/- 0.01 |
| | Upper left | 0.05 +/- 0.03 | 1.29 +/- 0.02 |
| | Lower left | 0.07 +/- 0.03 | 1.34 +/- 0.06 |
| | Lower right | Failed visit | Failed visit |
| F200W | Center | 0.06 +/- 0.01 | 1.63 +/- 0.14 |
| | Upper right | 0.04 +/- 0.01 | 1.48 +/- 0.13 |
| | Upper left | 0.05 +/- 0.01 | 1.51 +/- 0.03 |
| | Lower left | 0.05 +/- 0.01 | 1.52 +/- 0.08 |
| | Lower right | Failed visit | Failed visit |
| F356W | Center | 0.03 +/- 0.00 | 1.97 +/- 0.02 |
| | Upper right | 0.01 +/- 0.01 | 1.96 +/- 0.07 |
| | Upper left | 0.04 +/- 0.01 | 1.98 +/- 0.00 |
| | Lower left | 0.03 +/- 0.00 | 2.00 +/- 0.07 |
| | Lower right | Failed visit | Failed visit |

The EE profile for the F356W PSF matches perfectly for all the 4 locations on the detector and is consistent with the WebbPSF profile, and there is no evidence for spatial variation of PSF from the NIS-022 program over the detector field of view. The effect of undersampling on the fractional energy contained in the central pixel is shown in Figure 7 which zooms in on the EE curves, showing the central 20 pixels. The fractional energy variation at the different locations is only seen for the shorter wavelengths and only at radii of ≤ 1 pixel, which is consistent with being due to the peak of the PSF being offset from the center of the pixel (similar to what is seen in Figure 2, see §4.1). In the case of the F356W filter, the PSF is close to being Nyquist-sampled and the intensity in the central pixel is by far not as sensitive to where the peak falls on the central pixel.

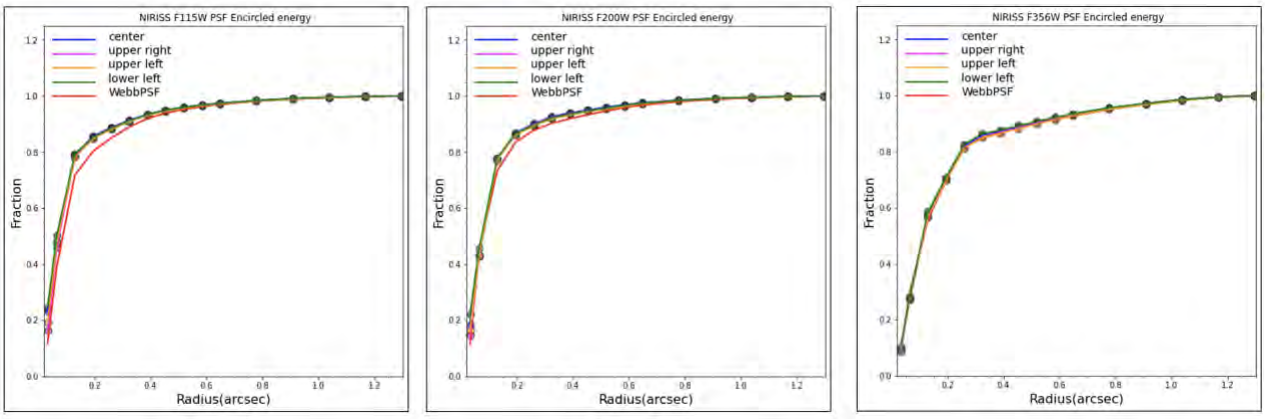


**Figure 6**: **The encircled energy curves from observation #2 of NIS-022 which looks at the spatial variation of the PSF across the detector. Filters are mentioned at the top of each panel and the EE radial profile at each position is shown in different color as indicated. Data points represent photometry of J125701.95+220415.5. For comparison, the EE profile for the WebbPSF model for the center position in each filter is also shown.**

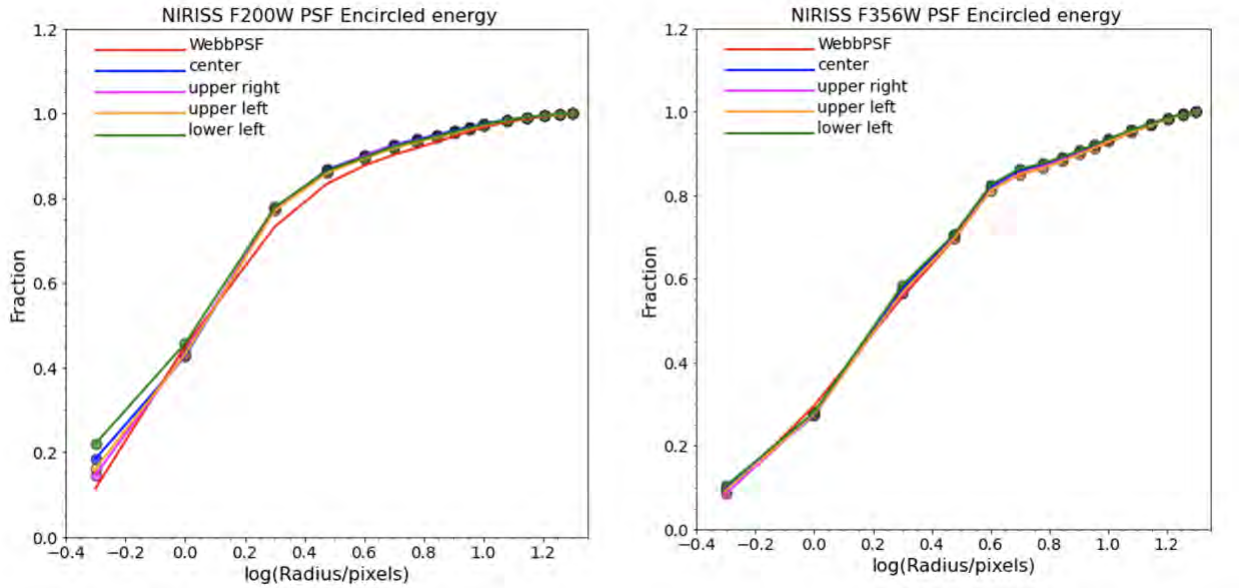


**Figure 7**: **Same as Figure 6, showing a zoom-in of the EE radial profiles in the central pixels to illustrate how the undersampling at shorter wavelengths (left) affects the measured encircled energy compared to the nearly Nyquist-sampled PSF at longer wavelengths (right).**

## 6 EEs from flatfielded vs. resampled images

While image combination and resampling into an undistorted image via the drizzle method (Fruchter & Hook 2002) can lead to a significant improvement of the effective spatial resolution of images with intrinsically undersampled PSFs, the images taken for this program are not really suitable to test the effect of this on EEs for the inner few pixels in detail. This is because (a) we only used 2 dithers per filter for this program in order to keep the duration of this commissioning program reasonably short, while severely undersampled images like those of NIRISS need at least 4 dithers to yield significant improvement in this context (see Goudfrooij 2015); and (b) the exposures were deep enough to achieve sufficient S/N in the outer regions of the PSF. The consequence of the latter was that the peak pixels of the star saturated within typically only 2-4 groups up the integration ramp depending on the filter and where the PSF is centered relative to pixel boundaries. When this happens for exposures involving undersampled PSFs, one often has to deal with issues related to properly scaling the signal levels of the central few pixels of the PSF during the resample step when using the default weight_type = 'ivm' weighting method. These issues arise because the distribution of signal levels among the central few pixels depends strongly on the location of the PSF centroid relative to pixel boundaries, which can lead to a significant difference of the number of "valid" groups in the peak pixel (meaning groups that are unsaturated and not affected by charge migration) among the different dithers. This effect leads to a slight broadening of the PSF in the resampled combined image (unless one uses parameter values customized to the individual case in the "jump detection" step of the Detector1 stage of the pipeline), and will be described in more detail in a separate report. Due to this situation, we use the individual flatfielded images (i.e., the level-2 products of the JWST pipeline) to measure the EEs for this report and to determine the aperture correction reference files from the commissioning

data (see §7 below). EEs at small measurement apertures will be derived from drizzled images taken using several dithers per filter during Cycle 1 calibration, which is expected to yield updated aperture correction reference files.

To illustrate the quality of EEs after image combination of the two dithers using the drizzle method and to compare them with the EEs from the individual exposures, we run the Image3 pipeline on the datasets for all filters separately using default settings and measure aperture photometry using pgphotdefs.pgapphot[1] followed by measurement of the EEs using EEnormalize_nis.py on the resulting drizzled images as described above. Figure 8 compares the run of EEs measured from the level-3 products (i.e., the _i2d.fits files) with those from the level-2 products (the _cal.fits files) which were shown before in Figure 3.

## 7 Reference File Creation

The results from commissioning program NIS-22 were used to create the APCORR pipeline reference file for imaging in CRDS from in-flight data. This reference file is used to correct the aperture photometry in the "source_catalog" step of the JWST pipeline for signal loss outside the measurement aperture.

A description of the creation procedure for this file along with the associated Python scripts and other relevant files is available in the NIRISS GitLab area on the APCORR reference file, and will not be repeated here.

## 8 References

Goudfrooij, P., 2015, "NIRISS Dither Patterns for the WFSS and Imaging Observing modes", JWST Technical Report JWST-STScI-004466

Goudfrooij, P., 2022, "Accuracy and Precision of Centroid Algorithms in the photutils Python package for NIRISS Point Spread Functions", JWST Technical Report JWST-STScI-008116

Perrin, M., et al., 2012, "Simulating Point Spread Functions for the James Webb Space Telescope with WebbPSF", Proc. SPIE, Vol. 8442, article id. 84423D

Perrin, M., et al., 2014, "Updated Point Spread Function Simulations for JWST with WebbPSF", Proc. SPIE, Vol. 9143, article id. 91433X

[1] pgapphot is very similar to pgphotdit2 described in §3, except that it acts on single (non-dithered) images.

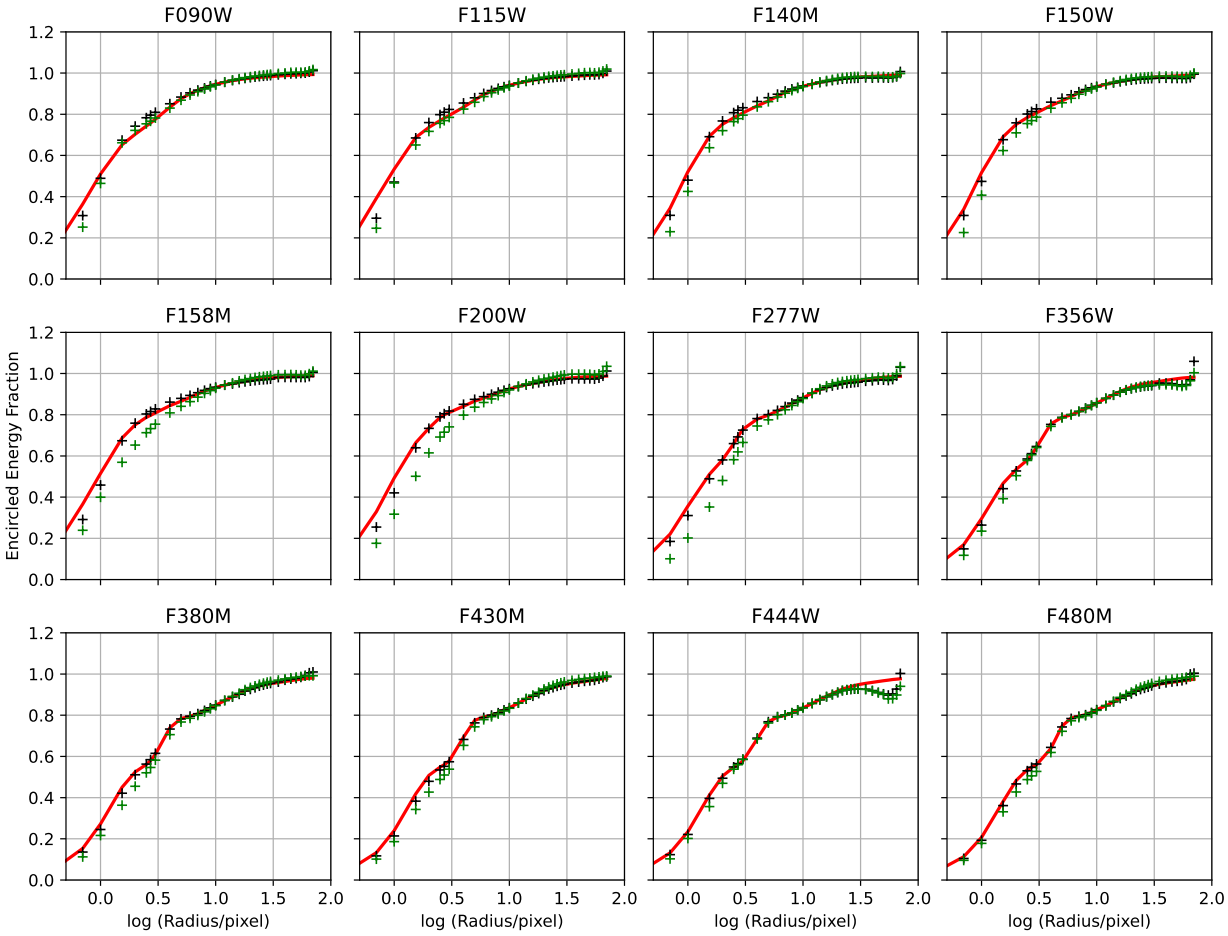


**Figure 8: the black symbols and red line are the same as in Figure 3. The green symbols represent the EE measurements on the level-3 pipeline products (i.e., the combined, resampled images). Note that the PSFs in the latter products are somewhat less centrally peaked than those for the level-2 products (i.e., the individual flat-fielded images) for this dataset, which is sub-optimal for producing high-quality combined images, especially for the filters with short pivot wavelengths (see text for details). Hence, we use EEs measured from the level-2 products to produce the APCORR reference file from the commissioning data.**